Kinetically evolving irradiation-induced point defect clusters in UO_2 by molecular dynamics simulation

Dilpuneet S. Aidhy
Department of Materials Science and Engineering, University of Florida, Gainesville, Florida 32611, USA

Paul C. Millett, Tapan Desai, and Dieter Wolf
Materials Sciences Division, Idaho National Laboratory, Idaho Falls, Idaho 83415, USA

Simon R. Phillpot*
Department of Materials Science and Engineering, University of Florida, Gainesville, Florida 32611, USA
(Received 23 April 2009; revised manuscript received 1 July 2009; published 18 September 2009)

The evolution of irradiation-induced point defects in UO_2 is captured in molecular dynamics simulations. The approach used circumvents their creation during the ballistic phase of a traditional collision-cascade molecular dynamics simulation but rather focuses on their kinetic evolution. The simulations reveal that in the absence of defects on the cation sublattice, the defects initially present on the anion sublattice recombine and annihilate completely during equilibration. However, in the simultaneous presence of defects on both sublattices, Schottky defects are formed, thereby sequestering the oxygen vacancies. The resulting excess oxygen interstitials form cuboctahedral clusters, whose existence has previously been identified experimentally but whose generation mechanism has not been determined. It is concluded that the cation sublattice is primarily responsible for the radiation tolerance or intolerance of the material.

DOI: 10.1103/PhysRevB.80.104107 PACS number(s): 61.80.Jh, 81.05.Je

I. INTRODUCTION

Fluorite-structured UO_2 is the most widely used of all nuclear fuels. High-energy particle irradiation in materials causes damage by creating point defects, the clustering of which can form defect structures such as small clusters, voids, and stacking faults, ultimately leading to material failure. The damage tolerance of a material depends not only on the number of defects created during irradiation but also on their long-time kinetic evolution; understanding the complete evolution of defects is therefore very important. Experimentally however, it is difficult to capture the irradiation-induced short time-scale atomistic processes; computer simulations are particularly adept at capturing such dynamical processes.[1–4]

Under oxidizing conditions, UO_2 readily accommodates O interstitials to form UO_{2+x}. Ultimately these interstitials lead to a transformation to the β-U_4O_9 phase.[5] While a unit cell of β-U_4O_9 is 64 times larger than fluorite, the "typical cell" closely resembles that of fluorite. In particular, the uranium ions occupy positions similar to those in fluorite while the excess oxygen ions are accommodated in cuboctahedral (COT) clusters.[6,7] The COT cluster contains 12 oxygen atoms rather than eight, as in a unit cell of fluorite. Under irradiation of UO_2, there can be a local increase in the oxygen interstitial concentration near the damage site. Under these conditions, it is possible that COT-cluster formation may cause a local phase transformation to the U_4O_9 structure.

In this work, we use molecular dynamics (MD) simulations to elucidate the evolution of irradiation-induced point defects in UO_2, including the formation mechanism of COT clusters in the fluorite matrix, by using a methodology that captures the kinetic evolution of the irradiation-induced point defects.

II. SIMULATION METHODOLOGY

A. Kinetically evolving irradiation-induced defects method

Atomistic simulations have been shown to capture two important phases of radiation damage. First, the "ballistic phase" involves the formation of cascades of defects through a primary knock-on atom (PKA); second, the "kinetic phase" involves the diffusion-controlled dynamical evolution of these defects. During the ballistic phase, large numbers of point defects are created due to the impact of a PKA. The atoms are displaced from their lattice sites, thereby forming vacancies and interstitials (Frenkel pairs). This phase typically lasts only for a few picoseconds. The kinetic phase, during which most of the interstitials recombine with the vacancies, lasts much longer. There may be a few interstitials that are not able to quickly recombine with vacancies. Their ultimate fate then depends on the diffusion-controlled kinetics under which they can either eventually recombine with the vacancies, interact with the microstructure, or evolve into clusters. It is thus this kinetic phase that determines the longer time, experimentally accessible behavior of the material. While interstitial-vacancy recombination promotes radiation tolerance of the material, their evolution into clusters results in potentially long-lived radiation damage that could be detrimental to the performance and lifetime of the material. Understanding the defect evolution during the kinetic phase therefore becomes very important for engineering radiation tolerant materials.

Conventional radiation-damage MD simulations using the PKA approach well capture the formation of the defects. However, because of the high energy of the initial PKA, the system sizes required are very much larger than the volume in which the surviving point defects kinetically evolve. As a result, the sizes of the simulations are typically not large

enough nor contain a high-enough concentration of defects to allow the formation of complex defect structures in the available MD time. Recently, simulations involving conventional damage-cascade MD followed by temperature-accelerated dynamics (TAD) (Ref. 8) have been used to extend radiation-damage simulations to the experimental time scale. Interestingly, these simulations have shown the development of more complex defect structures than seen in previous conventional cascade simulations. Moreover, combined MD-TAD simulations on MgO (Ref. 8) have shown that the defect evolution during the kinetic phase is largely independent of the initial damage during the ballistic phase. In addition, it has been shown in UO_2 that the initial PKA direction has little effect on the final defect evolution.[9] Together, these observations strongly suggest that a detailed understanding of the ballistic phase is not necessarily a prerequisite for understanding the long-term evolution of the irradiated system.

Here, we use a methodology that circumvents the ballistic phase and focuses entirely on the evolution of defects. This approach allows us to observe defect evolution under different defect environments and reveals the governing mechanism in the radiation tolerance of UO_2. In this method, at the beginning of each simulation we create a specified number of point defects in a high-temperature ($T=1000$ K) equilibrated system. To avoid uninteresting spontaneous interstitial-vacancy recombination events, the vacancies and interstitials are separated by a distance of $5a_o$, which is more than the recombination radius. Because they cannot mutually annihilate, there is no constraint on the vacancy-vacancy and interstitial-interstitial distances. The system is then allowed to equilibrate at high temperature and the diffusion-controlled kinetic evolution of the system is followed. This method has features in common with a method by Crocombette.[10] In both methods, rather than following a particular PKA, cation Frenkel pairs (FPs) are created by hand and their evolution is followed. However, here the effects of anion FPs alone and the combined effects of anions and cations are also considered. As we shall see, kinetic evolution of oxygen FPs forms the most important part of this study. Crocombette *et al.* added FP successively; in this work, all FPs are introduced at the beginning of the simulation, after which the defects interact without interference. Finally, all of the simulations presented here are performed at 1000 K in contrast to the simulations of Crocombette *et al.*, most of which were performed at 300 K.

When this method was applied to MgO,[11] we were able to reproduce the clusters that were observed from the combined radiation damage and MD-TAD simulations.[8] Moreover, by focusing entirely on the kinetic phase of radiation damage, it allowed us to better understand the defect recombination and clustering mechanism in MgO. Here, we apply this methodology to UO_2 to capture new details of the defect evolution.

B. Interatomic potential and molecular dynamics method

The interactions between the ions are described by a pair potential. Here, the short-range atomic interactions are captured using the potential form provided by Ida[12] with parameters taken from Basak *et al.*[13] In addition to the widely implemented Buckingham-type form for ionic materials, the Bushing-Ida potential form also includes a Morse term that introduces a "covalent" component. Due to the assumption of partial covalency, the ionic charges are given nonformal values, which take into account partial charge transfer between the ions. The Basak potential parameters were chosen as they predict a correct order of Schottky-defect energies of trivacancies ($V_O^{\bullet\bullet}-V_U^{''''}-V_O^{\bullet\bullet}$),[14,15] which is crucial for a physically appropriate representation of the defect properties. The long-range electrostatic interactions are calculated using the direct-summation method of Wolf *et al.*[16] In this method, the Coulombic energies and forces are truncated at a fixed cutoff radius with charge compensation on the surface of the truncation sphere. This method has been applied to various materials[16,17] and has been demonstrated to be accurate. It is also computationally very efficient as the computational load scales linearly with the system size.

The melting point for this interatomic description of UO_2 has been determined to be $\sim 3450 \pm 50$ K,[18] which is in fair agreement with the experimental value of 3100 K.[19,20] Likewise, the oxygen sublattice ordering temperature for this potential has been determined to be 2200 K,[18] which is also in fair agreement with the experimentally obtained value of 2600 K.[21] All the simulations were carried out at a temperature of 1000 K, i.e., well below the melting and sublattice melting temperatures. At this temperature, the oxygen interstitials and vacancies have high diffusivities, whereas their uranium counterparts are much less mobile due to their high migration energies; this temperature is also representative of the temperature range of 800–1600 K present in a typical fuel pellet.

We have carried out all simulations on a UO_2 single crystal containing 96 000 ions with periodic boundary conditions applied in all three dimensions. The trajectories of the ions are calculated using a fifth-order Gear predictor-corrector method with an MD time step of 0.5 fs. This time step is small enough to conserve energy over several thousand MD steps in microcanonical ensemble test runs. To capture as much of the defect evolution as possible, all the simulations are carried out for more than 1 ns. The point defects are identified by comparing the defect structure with the initial structure containing no defects. If any lattice site does not contain an atom within a spatial cutoff radius of 1 Å, or an interstitial site is filled within a spatial cutoff radius of 1 Å, the site is identified as a vacancy or an interstitial, respectively.

III. DIFFUSION-CONTROLLED KINETIC EVOLUTION OF DEFECTS

We first ensure that no defects are spontaneously formed during equilibration. This is done by simply equilibrating a perfect crystal at 1000 K for 1 ns. Given that the oxygen Frenkel pair formation is 6.0 eV for this potential,[14] a defect concentrations of 1.6×10^{-26} would be expected for the number of atoms in the simulation. Consistent with this, the perfect crystal does not spontaneously generate defects; this structure is used for rest of the simulations.

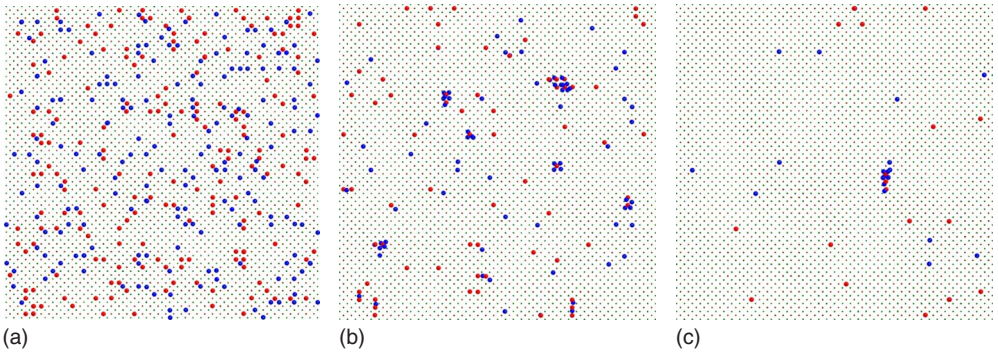

FIG. 1. (Color online) Evolution of the point defects present only on the O sublattice: red for vacancies and blue for interstitials snapshots taken at (a) $t=0$ ps, (b) $t=40$ ps, and (c) $t=300$ ps. Initially 200 FPs were randomly distributed on the oxygen sublattice. After 40 and 300 ps, only 78 and 21 O FPs are left behind. The O FPs annihilate by a vacancy-interstitial recombination mechanism with no clustering of the defects.

A. Frenkel pair defects on a single sublattice

In order to provide a benchmark against which to compare our results, we first focus on the evolution of a system in which the FPs are created on only one sublattice: either the O or the U sublattice. Taking the oxygen case first, FPs are created by removing a random O atom from its cubic sublattice site and placing it at an octahedral interstitial site. At the beginning of the simulation, 200 FPs are created in the previously equilibrated system. A snapshot of the initial structure with O FPs is shown in Fig. 1(a). The system is then allowed to thermally re-equilibrate at 1000 K. The snapshots of the subsequent time evolution of the O FPs to $t=40$ and 300 ps are shown in Figs. 1(b) and 1(c), respectively. Due to the low migration energies of both the O interstitials and the vacancies,[14] the O FPs have high diffusivities. As evident from Figs. 1(b) and 1(c), the number of O FPs decreases with increasing time. The number of O FPs is shown as red triangles in Fig. 2. By 1400 ps, only four O FPs are left in the system. Eventually, all of the O FPs recombine

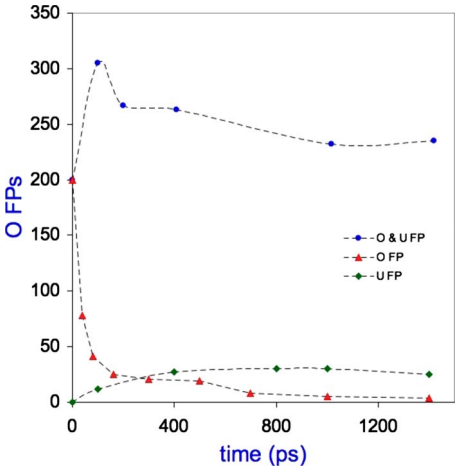

FIG. 2. (Color online) Total number of O FPs present when the system is initialized with three different defect conditions: (1) defects present only on O sublattice (red triangles); (2) defects present only on U sublattice (green diamonds), and (3) defects present on both O and U sublattices (blue circles); in contrast to (1), in other two cases, new FPs are created on the O sublattice.

by vacancy-interstitial recombination; no interstitial-interstitial or vacancy-vacancy clustering is observed. This demonstrates that, in the absence of defects on the cation sublattice, the O sublattice is completely healed within a few picoseconds, resulting in no long-lasting damage to the material.

In contrast to the above expected result, the simulation of FPs on the U sublattice alone yields a surprise. We create 200 FPs on the U sublattice. The initial snapshot of the system with defects is shown in Fig. 3(a); snapshots at later times are shown in Figs. 3(b) and 3(c). Since, the U interstitials and vacancies have very high migration energies,[14] recombination events are less frequent than in the O case; of the initial 200 U FPs, 160 U FPs are still present after 1700 ps. What was not expected, however, was that the high concentration of the defects on the U sublattice nucleates O FPs (shown as the diamonds in Fig. 2). Starting from no O FP at $t=0$ ps, there is a gradual increase in the number of O FPs; this peaks at ~600 ps with a total of ~30 FPs and then slowly levels off; however, even after 1700 ps about 20 O FPs survive [Fig. 3(b)]. Although most of the vacancies and interstitials that make up individual O FPs remain close to each other (within $2a_o$), some of them diffuse far enough from their counterpart that they are unlikely to undergo rapid recombination. Indeed, some of the defects are no longer isolated but, as seen in Fig. 3(c), actually form clusters. A detailed analysis of these structures is given below. What is most noteworthy here, however, is the observation that the presence of the defects on the U sublattice leads to the spontaneous formation of O FPs, whose diffusion controls the longer time evolution of the system.

B. Frenkel pairs on both U and O sublattices

The above simulations are rather artificial because a material under irradiation never produces defects on one sublattice alone. We thus turn our attention to a more realistic radiation-damage situation; in this simulation, we simultaneously create 200 FPs on both the U and O sublattices. As in the previous simulations, all of the interstitials are created on the empty octahedral sites of the fluorite unit cell. A snapshot of the random defect distribution in the system at t

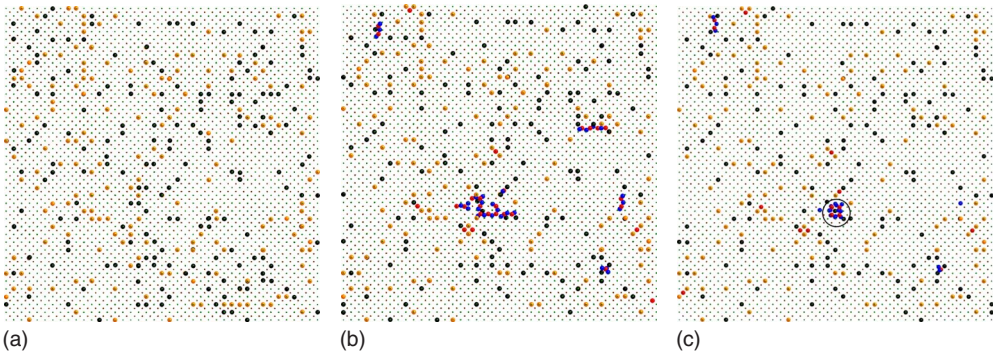

FIG. 3. (Color online) Evolution of the point defects present only on the U sublattice. Snapshots taken at (a) $t=0$ ps, (b) $t=1000$ ps, and (c) $t=1700$ ps. (a) Initially 200 FPs were randomly distributed on the uranium sublattice. (b) Due to the large number of U defects, some new O FPs are created which diffuse with time. The interstitials diffuse and form a cluster shown as circled in (c). (See Fig. 6 for details on cluster).

$=0$ ps is shown in Fig. 4(a). During equilibration the U interstitials and vacancies are largely immobile, as expected based on the simulations on the U sublattice alone, with only a few diffusing during the entire simulation (within first 1000 ps, only 15 U FPs have recombined). Snapshots of the system at $t=40$ ps and 1000 ps are shown in Figs. 4(b) and 4(c). In contrast to the results for FPs on the O sublattice alone, a substantial number of defects remain at the end of the simulation. The time evolution of the O FP concentration shows a large increase within the first 100–150 ps, followed by a slow decline. Instead of almost complete elimination of the O FPs at the end of the simulation, their number is actually larger than at the beginning of the simulation. This indicates that there are two different phenomena taking place simultaneously. First, random diffusion of the vacancies and interstitials results in elimination events by recombination. Second and more interesting, and responsible for the sharp increase in Fig. 2, is the spontaneously formation of *new* O FPs. These are created by an O ion spontaneously moving from the crystal lattice site to a nearby interstitial site. The surviving original O FPs and the newly created O FPs together evolve into clusters while the O interstitials form COT clusters, the O vacancies form Schottky defects with the U vacancies. The structures of these clusters are discussed in detail below.

Considered together, the above three simulations illustrate two important points. First, U FPs influence the radiation tolerance of UO_2; the presence of U FPs not only prevents O FP recombination but in certain cases also contributes to the creation of new FPs. This in turn shows that the radiation tolerance of UO_2 decreases if the U FPs remain in the system. Second, from the methodology viewpoint, this approach of selectively creating defects on different sublattices provides insights into the defect-evolution mechanisms.

C. Vacancy clustering: Schottky defects

A Schottky defect in UO_2 involves two O vacancies and one U vacancy. The evolution of vacancies into Schottky defects takes place in both systems with defects only on the U sublattice (through the spontaneous creation of O FPs) and systems with defects simultaneously present on both O and U sublattices. In both cases, the process involves the diffusion of the mobile O vacancies to the essentially immobile U vacancies. A snapshot of a Schottky defect is shown in Fig. 5. Separate static calculations have shown that a Schottky defect has a much lower energy than a $V_O^{\bullet\bullet}-V_U^{''''}$ dicluster with a distant O vacancy. The system with completely separated vacancies has a higher energy yet. As a result, the Schottky defect created by diffusion is extremely stable. While most

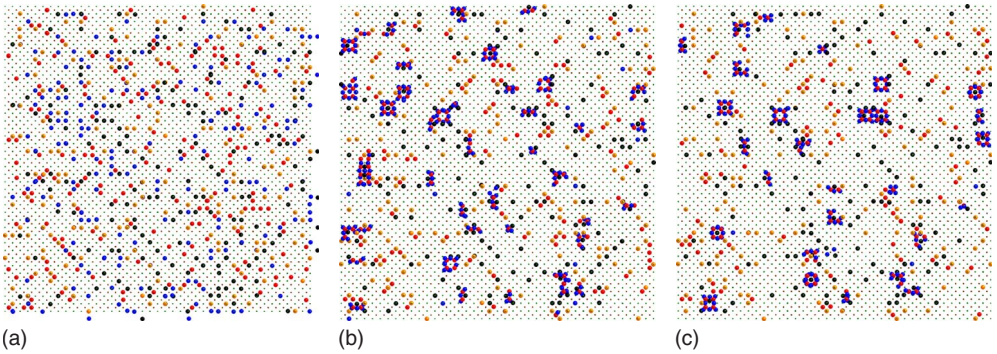

FIG. 4. (Color online) Evolution of the point defects simultaneously present on both O and U sublattices: orange and black for uranium vacancies and interstitials. Snapshots taken at (a) $t=0$ ps, (b) $t=40$ ps, and (c) $t=1000$ ps. Initially 200 FPs were randomly distributed on each sublattice. As time progresses, most of the O interstitials aggregate to form clusters. The U vacancies and interstitials are almost immobile and do not participate in clustering directly.

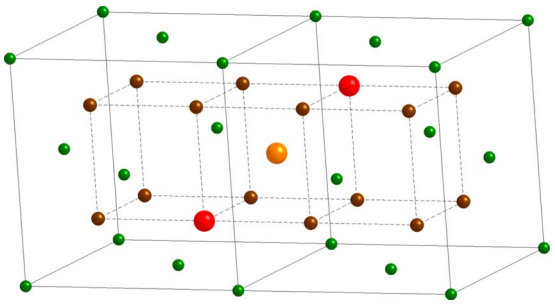

FIG. 5. (Color online) Snapshot of Schottky-defect formation. Two O vacancies tend to align in ⟨111⟩ direction around a U vacancy.

of the Schottky defects form as $V_O^{\bullet\bullet}-V_U^{''''}-V_O^{\bullet\bullet}$ along ⟨111⟩ (Fig. 5), some form along ⟨110⟩. Regardless of the specific orientation, these Schottky defects sequester O vacancies, thereby making them unavailable for vacancy-interstitial recombination events. This leads to the O interstitials, whose potential recombination partners are sequestered in Schottky defects, forming complex interstitial-defect clusters.

D. Interstitial clustering: Cuboctahedral clusters

The O interstitials form COT clusters containing 12 O interstitials and eight O vacancies inside a single UO_2 unit cell. Such interstitial clusters have been previously observed experimentally in oxygen-rich UO_2 systems[6,7,22] and have been found to be stable in electronic-structure calculations.[23] These simulations allow the dynamics of the formation process itself to be determined.

Two types of COTs, distinguished by having a vacant (COT-v) or occupied (COT-o) octahedral site at their center have previously been identified (as discussed in Ref. 23). In the COT-o clusters, the octahedral site is occupied by an oxygen ion. In our simulations, we find that a U ion can also occupy the octahedral site inside the COT cluster (COT u). Figures 6(a)–6(c) show the COT-v, COT-o, and COT-u clusters, respectively, as spontaneously formed in our simulations. In all of these clusters, the U sublattice (atoms in green) remains undisturbed; by contrast the cubic O sublattice begins to break down. In particular, rather than eight O ions occupying the corners of the simple-cubic sublattice, there are 12 O interstitial ions and no ions at all occupying the original cubic sublattice sites. A crystallographic analysis of the COT clusters is given elsewhere.[6,7]

The formation of such clusters would be extremely unlikely if it required all of the O ions to converge on a single unit cell at the same time. Indeed, our simulations show that the COT forms in a progressive manner, as illustrated in Fig. 7 for a COT-u cluster. Figure 7(a) is a snapshot at $t=3$ ps of a unit cell containing a U interstitial at its center. At this time, all the O sublattice sites are occupied. At $t=4$ ps, one diffusing O interstitial enters the unit cell; as a result two O ions move from their lattice sites to interstitial sites, creating the structure shown in Fig. 7(b). The unit cell now contains two O vacancies and three O interstitials. In Fig. 7(c) at $t=20$ ps, another O interstitial enters the unit cell, which further creates two O FPs. As a result, there are four new O FPs created in the unit cell by the addition of two O interstitials. Similarly, further addition of two more O interstitials creates four more O FPs, thereby completing the COT structure [Figs. 7(d) and 7(e)].

Figure 7(f) shows that the energy of the system decreases when the distributed O interstitials progressively form the COT cluster. The other two clusters, COT v and COT o, form via the same clustering mechanism and with similar energetics. This formation mechanism of a COT cluster therefore explains the sharp increase in the number of the O FPs as observed in Fig. 2. For every complete cluster that appears in the system, there is an increase of 8 O FPs with all of these new FPs appearing from the O displacements within a cluster. These new FPs are formed only because of an extra oxygen ion entering the unit cell: their isolated formation has not been observed.

The O interstitial-cluster formation is stabilized by the simultaneous formation of Schottky defects since the U vacancies pin the O vacancies in Schottky-defect clusters. This forces the O interstitials to either remain isolated or form some sort of cluster. To illustrate this directly, we performed simulations on systems containing only interstitials: eight extra O interstitials plus four U interstitials for charge balance. A snapshot of the system at $t=140$ ps is shown in Fig. 8 (U *interstitials not shown*). The initially well-separated O interstitials diffuse and evolve into COT clusters. In Fig. 8, one of the interstitial clusters has completely formed while another is in the process of construction. A similar scheme is applied to understand the evolution of the independent vacancies. Eight O vacancies and four U vacancies are created in the

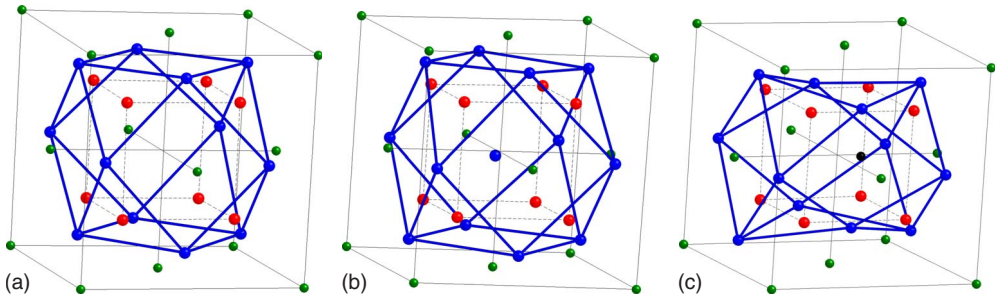

FIG. 6. (Color online) Schematics of three different kinds of COT clusters as seen in Fig. 2 differentiated by filled or empty octahedral site. The interstitials displace the lattice oxygen atoms, thereby creating 12 O interstitials and eight O vacancies. The U lattice remains undisturbed. (a) An empty COT cluster, (b) O-filled COT cluster, and (c) U-filled COT cluster.

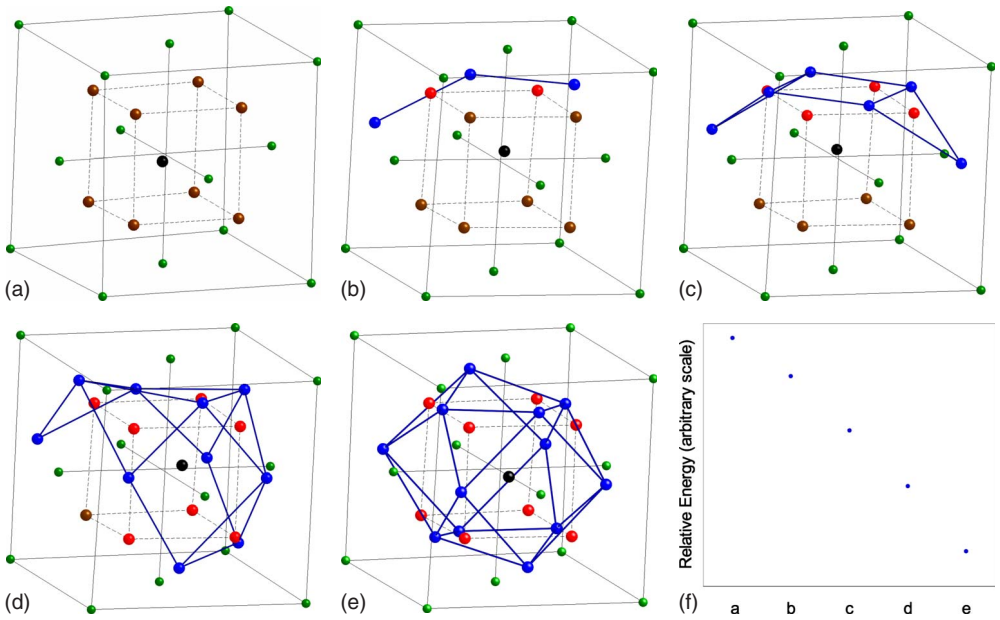

FIG. 7. (Color online) Snapshots showing progressive formation of COT cluster, as seen in an MD simulation. (a) A fluorite unit cell containing a U interstitial atom at the central octahedral site at $t=3$ ps. (b) At $t=4$ ps, a diffusing O interstitial enters the unit cell. Two oxygen atoms are knocked from their lattice site, forming two O vacancies and two additional O interstitials. (c)–(e) are snapshots at $t=20$, 120, and 250 ps. For every additional O interstitial entering the unit cell, two additional O atoms are knocked off from their lattice sites. (f) The relative decrease in the energy of the system as the cluster is formed.

system. The snapshots of the initial structure at $t=0$ ps and the equilibrated structure at $t=280$ ps are shown in Fig. 9. In Fig. 9 two Schottky clusters have already formed and one is in the process of formation.

E. Evolution of disproportionately defected systems

Up to this point, we have illustrated the point defect clustering process and the independent evolution of vacancies and interstitials. We now present the dependence of the evolution of O FPs on that of U FPs. To do this, we examine the O FP evolution in a disproportionately defected system with a large number of O FPs (200) but a small number of U FPs (50). As Fig. 10 shows, by 200 ps there is a significant decrease in the number O FPs, which then levels off by about 500 ps. We perturb the system with the hope of stimulating further interactions by creating a further 200 O FPs. As evidenced by the first peak in the plot, the system again equilibrates for another 500 ps with most of the O FPs again recombining leaving behind almost the same number of O FPs as were observed after the first 500 ps. At this point (1000 ps), we perform two further simulations on the equilibrated system. In the first, we again add yet another 200 O FPs to the system. In the second, we simply allow the 1000 ps system to continue to equilibrate undisturbed (i.e., without any addition of O FPs). After an additional 500 ps, the two sys-

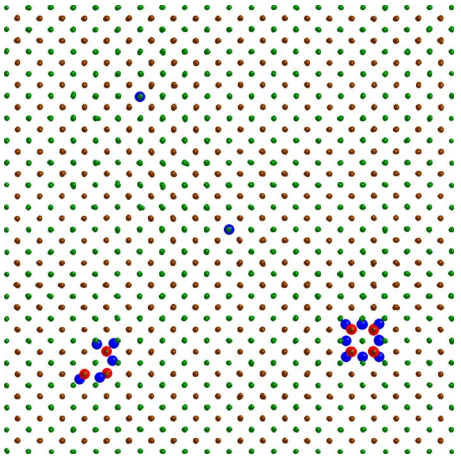

FIG. 8. (Color online) Clustering of oxygen interstitials in the absence of vacancies. Initially four U and eight O interstitials were added to the system. The O interstitials diffuse and form COT clusters. One cluster is complete while the second one is in the process of formation. The U interstitials (not shown here) remain immobile.

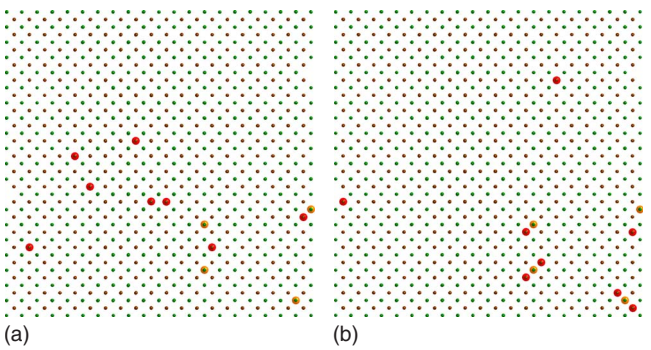

FIG. 9. (Color online) Snapshots showing clustering of U and O vacancies. (a) At $t=0$ ps, four U and eight O vacancies are created in the system. (b) O vacancies diffuse and cluster around U vacancies forming a ⟨111⟩ oriented cluster. Two ⟨111⟩ aligned clusters have formed by $t=280$ ps.

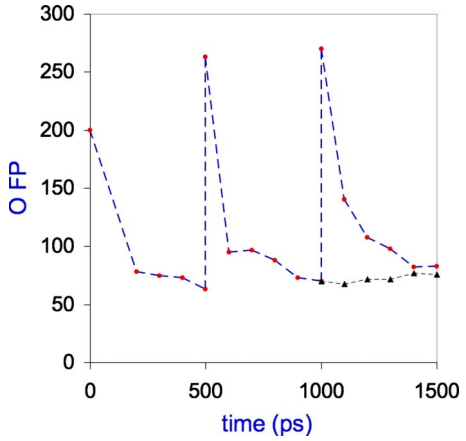

FIG. 10. (Color online) Evolution of the number of O FP in a system initially containing 200 O FPs and fixed U FPs. After 500 ps, the number of O FPs levels off to ~60. Another 200 O FPs are added at 500 ps and 1000 ps shown by two peaks. In both cases, the number of O FPs again level off to an equilibrium value. Evolved system at 1000 ps was also separately equilibrated for 500 ps (black triangle). Each case leads to almost the same number of O FPs at $t=1500$ ps.

tems have almost identical numbers of O FPs. We thus conclude that the equilibrated O FPs concentration depends entirely on the U FPs concentration in the system.

To confirm this relationship between the number of O FPs and U FPs, we perform five different simulations with systems initially containing 100 O FPs but varying number of U FPs, i.e., 10, 20, 30, 50, and 70. Figure 11(a) gives the time dependence of the number of O FPs for each system. As the initial U FPs concentration is increased, the number of surviving O FPs also increases. For illustration, we compare the systems containing 10 and 70 U FPs. At $t=0$ ps, both the systems contain 100 O FPs. However, with time, the number of O FPs differs significantly between two systems. For the system containing ten U FPs, the O FPs number drops to 34 by $t=500$ ps and then to 15 at $t=1000$ ps. Due to a very low concentration of U FPs in this system, most of the O vacancies and interstitials annihilate by recombination. The number of O FPs has been found to level of by $t=800$ ps illustrating that no further O FP recombination takes place. The

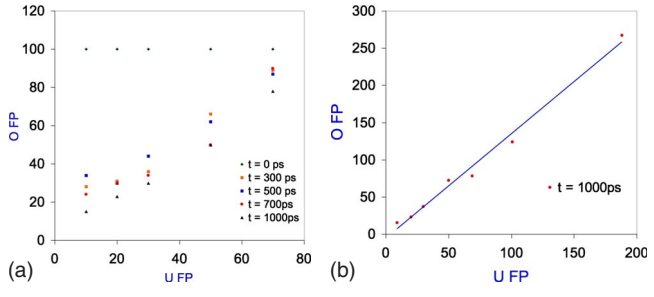

FIG. 11. (Color online) Number of O FPs with increasing time a function of number of initially created U FPs. (a) Initially, 100 O FPs were created on each of six different systems containing 10, 20, 30, 50, and 70 U FPs. (b) Linear dependence of the concentration of surviving O FPs on the U FPs in a well-equilibrated system ($t=1000$ ps). (Straight line is shown as a guide to the eye.)

system with 70 U FPs displays a different evolution. In this case, the data points for all five different time periods are concentrated close to one another and near to the high end of the plot. This illustrates that not many recombination events take place. By $t=500$ ps, only 13 O FPs have recombined and 87 survive. Even with additional time, the number of FPs does not decrease much, with 78 FPs surviving. Unlike the recombination mechanism that is dominant in the ten U FPs (low-concentration) system, here the system forms new FPs. This shows that an increasing concentration of U FPs tends to stabilize an increased concentration of O FPs in the system. Further, if the O FPs concentration is not sufficient for the given U FPs concentration, the system responds by creating new O FPs as also seen previously in Fig. 4. The data in Fig. 11 for the other systems also shows an increase in O FPs as the U FPs are increased. By further extending the data to higher concentrations of around 200 U FPs, it is found that in a well-equilibrated system ($t=1000$ ps), the number of O FPs depend linearly on the number of U FPs as shown in Fig. 11(b).

IV. DISCUSSION

The simulation approach used here provides a good understanding of the kinetic phase of defect evolution and thus complements the collision-cascade simulation method. It can be argued that it is predicated on an unrealistically large concentration of defects. While this may be true when averaged over time and space, statistically it can be expected that such high defect concentrations will on occasion be generated over some spatial region. Moreover, the resulting defect structures, unlike rapidly recombining point defects, will have a significant role in determining the true radiation performance of the material.

It is interesting to compare this UO_2 system with MgO. In both systems we observed[11] that if the defects are present only on one sublattice, the FPs quickly recombine, whereas if defects are present on both sublattices they form clusters. Further, not only is the defect evolution similar but in both systems the clusters are also in part stabilized by formation of new FPs. In UO_2, we have seen that new FPs form only on O sublattice which stabilize the COT clusters. In MgO, new FPs are spontaneously formed on both the Mg and O sublattices. This difference in the system evolution arises from the differences in crystallography and energetics of the two systems. In particular, the interstitial lattice in MgO has the same structure of parent rocksalt crystal structure, thereby supporting growth of defect clusters through the creation of the FPs required to provide any missing interstitial in the $(MgO)_4$ crystal structure. Moreover, since the MgO crystal lattice and interstitial lattices have the same structures, the extent and shape of the defect cluster is not limited. By contrast, the lattice of interstitial sites in UO_2 does not have the symmetry of the parent lattice. As a result, the defect clusters have a defined extent and shape: a COT within a single unit cell.

COT clusters are observed experimentally in oxygen-rich UO_2. It was shown by Murray and Willis[22] that the extra oxygen ions form COT clusters in systems with O:U ratio

greater than 2.13:1. The observation of COT clusters in stoichiometric UO_2 with no extra O interstitials has not been anticipated: it may be due to the high concentration of the interstitials in the system. This hypothesis is supported by our simulations on an interstitial only system (Fig. 8). However, the absence of clustering in the simulation beginning with O FPs alone illustrates that charge imbalance on the U sublattice also plays a very important role. From analysis of all the simulations above, a clear picture emerges that the defects on the U sublattice are primarily responsible for the radiation intolerance of the UO_2. A similar observation has also recently been made in pyrochlore-based materials,[24] for which the cation disorder was found to be the driving factor behind the oxygen disorder.

Andersson *et al.*[25] have recently used density-functional theory (DFT) calculations to predict the most stable defect cluster. They found split-quad interstitials to be the most stable O interstitial configurations in the hyperstiochiometric systems, followed by COT clusters. The least stables were found to be individual interstitials at octahedral sites. Our MD simulations also predict COT clusters to be more stable than individual interstitials; however, we have not observed split-quad interstitials in our simulations. This disagreement could be due to the limited materials fidelity of the empirical potential or could be due to the effect of temperature: the DFT calculations were performed at 0 K whereas the MD simulations are performed at very high temperatures.

An atomistic simulation is only as good as the potential that describes the interatomic interactions. We recall that the Basak potential used for these simulations has nonformal charges lower than the nominal valences of the ions. This introduces a degree of covalency to the system. By contrast, a number of other potentials use strictly formal charge model (i.e., U^{4+} and O^{2-}). Corresponding simulations of FP evolution using one of these formal charge potentials, the Busker potential, do not show COT-cluster formation. Further, a preassembled COT cluster quickly disintegrates when allowed to evolve using the Busker potential. These qualitatively different results for these two potentials arise from the difference in charges. In particular, the electrostatic repulsion among the like-charged interstitials is much higher for formal charges (Busker) than for partial charges (Basak). That both DFT calculations and experiment have shown the presence of COTs strongly suggests that a nonformal charge model is a better choice to model the defect evolution. This is also consistent with the conclusion of Govers *et al.*[14] that partial-charge models for UO_2 generally provide higher materials fidelity than formal charge models.

Finally, this study has been performed on single crystals. A corresponding study in the polycrystalline UO_2 is required to elucidate the point defect evolution in the presence of the grain boundaries (GBs). In the polycrystalline system, not only will the point defects annihilate by vacancy-interstitial recombination mechanism but they may also be eliminated at the GBs. We therefore expect that the kinetics of the cluster formation may be impeded. An understanding of GB sink/source strength therefore needs to be established to understand the effect of GBs on defect evolution.

ACKNOWLEDGMENT

The work of the UF team was supported by DOE NERI under Contract No. DE-FC07-07ID14833. The work of the INL team was supported through the INL Laboratory Directed Research and Development program under DOE Idaho Operations Office under Contract No. DE-AC07-051D14517V. We gratefully acknowledge support from the DOE/BES funded Computational Materials Science Network (CMSN) project on "Multiscale simulation of thermomechanical processes in irradiated fission-reactor materials." D.A. is grateful to Blas Uberuaga and David Andersson for useful discussions and for the hospitality of INL during the period that most of this work was performed.

*Corresponding author; sphil@mse.ufl.edu

[1] W. J. Phythian, R. E. Stoller, A. J. E. Foreman, A. F. Calder, and D. J. Bacon, J. Nucl. Mater. **223**, 245 (1995).
[2] K. E. Sickafus, L. Minervini, R. W. Grimes, J. A. Valdez, M. Ishimaru, F. Li, K. J. McClellan, and T. Hartmann, Science **289**, 748 (2000).
[3] T. D. de la Rubia, H. M. Zbib, T. A. Khraishi, B. D. Wirth, M. Victoria, and M. J. Caturla, Nature (London) **406**, 871 (2000).
[4] Y. Matsukawa and S. J. Zinkle, Science **318**, 959 (2007).
[5] B. T. M. Willis, Acta Crystallogr. **A34**, 88 (1978).
[6] D. J. M. Bevan, I. E. Grey, and B. T. M. Willis, J. Solid State Chem. **61**, 1 (1986).
[7] R. I. Cooper and B. T. M. Willis, Acta Crystallogr., Sect. A: Found. Crystallogr. **A60**, 322 (2004).
[8] B. P. Uberuaga, R. Smith, A. R. Cleave, G. Henkelman, R. W. Grimes, A. F. Voter, and K. E. Sickafus, Phys. Rev. B **71**, 104102 (2005).
[9] L. V. Van Brutzel, J.-M. Delaye, D. Ghaleb, and M. Rarivomanantsoa, Philos. Mag. **83**, 4083 (2003).
[10] J.-P. Crocombette, A. Chartier, and W. J. Weber, Appl. Phys. Lett. **88**, 051912 (2006).
[11] D. S. Aidhy, P. C. Millett, D. Wolf, H. Huang, and S. R. Phillpot, Scr. Mater. **60**, 691 (2009).
[12] Y. Ida, Phys. Earth Planet. Inter. **13**, 97 (1976).
[13] C. B. Basak, A. K. Sengupta, and H. S. Kamath, J. Alloys Compd. **360**, 210 (2003).
[14] K. Govers, S. Lemehov, M. Hou, and M. Verwerft, J. Nucl. Mater. **366**, 161 (2007).
[15] H. Y. Geng, Y. Chen, Y. Kaneta, and M. Kinochita, J. Alloys Compd. **457**, 465 (2008).
[16] D. Wolf, P. Keblinski, S. R. Phillpot, and J. Eggebrecht, J. Chem. Phys. **110**, 8254 (1999).
[17] P. K. Schelling, S. R. Phillpot, and D. Wolf, J. Am. Ceram. Soc. **84**, 1609 (2001).
[18] T. G. Desai, P. C. Millett, and D. Wolf, Acta Mater. **56**, 4489 (2008).
[19] R. A. Hein and P. N. Flagella, General Electric Report GEMP 578, 1968.
[20] J. P. Hiernaut, G. J. Hyland, and C. Ronchi, Int. J. Thermophys. **14**, 259 (1993).

[21] J. Ralph, J. Chem. Soc., Faraday Trans. II **83**, 1253 (1987).
[22] A. D. Murray and B. T. M. Willis, J. Solid State Chem. **84**, 52 (1990).
[23] H. Y. Geng, Y. Chen, Y. Kaneta, and M. Kinoshita, Phys. Rev. B **77**, 180101(R) (2008).
[24] A. Chartier, G. Catillon, and J.-P. Crocombette, Phys. Rev. Lett. **102**, 155503 (2009).
[25] D. A. Andersson, J. Lezama, B. P. Uberuaga, C. Deo, and S. D. Conradson, Phys. Rev. B **79**, 024110 (2009).